Journal of the Optical Society of Korea
Vol. 12, No. 4, December 2008, pp. 255-261

DOI: 10.3807/JOSK.2008.12.4.255

# Side-Coupled Asymmetric Plastic Optical Fiber Coupler for Optical Sensor Systems

Kwang Taek Kim, Deok Gi Kim, Woong Keun Hyun, and Ki Bum Hong

*Department of Optoelectronics, Honam University, 59-1, Seobong-Dong, Gwangsan-Gu, Gwangju 505-714, Korea*

Kiegon Im* and Se-Jong Baik

*Department of Physics, Chonnam National University, Gwangju 500-757, Korea*

Dae-kyong Kim and Hyun-yong Choi

*Korea Electronics Technology Institute, Digital Convergence Center, 1110-11, Oryong-dong, Buk-gu, Gwangju, 500-480, Korea*

(Received September 25, 2008 : revised October 27, 2008 : accepted November 10, 2008)

This paper reports a side-coupled asymmetric 1×2 plastic optical fiber coupler for an optical sensor system. The dependence of the optical power coupling ratio on the coupling angle and refractive index of the adhesion layer in both the forward and backward directions was examined based on the geometrical optics. It was confirmed experimentally that the coupling ratios can be optimized by controlling the coupling angle and refractive index of the adhesion layer. A maximum forward coupling efficiency > 93% was achieved.

*Keywords*: Plastic optical fiber, Plastic optical fiber coupler, Optical fiber sensor

*OCIS codes* : (060.2370) Fiber optics sensors; (060.1810) Couplers, switches, and multiplexers; (060.2340) Fiber optics components; (060.2370) Fiber optics sensors

## I. INTRODUCTION

An optical sensor system is generally composed of an optical source, a sensor element and an optical detector. In order to separate the optical sensor signal from the optical source, complicated optics, which are composed of several aligned optical components, such as mirrors, lenses and/or beam splitters, are often used in optical sensor systems. A coupler is used in optical communication and sensor systems to divide or combine the optical signals. The complicated optics in a sensor system can also be replaced by a simple fiber coupler.

Plastic optical fibers (POFs) are often used in the field of short distance optical communications and fiber optic sensors. The 1arge core size and high numerical aperture of the POF facilitates optical beam launching into the fiber from an external source as well as the connection between plastic fibers. POF couplers have been developed based on the side-polishing method [1,2], the fusion and pulling method [3], and the fiber mixing method [4]. However, these couplers are not suitable for separating the sensor signal from the optical source. The POF coupler in optical sensor systems requires the optical source beam to be delivered to the sensing tip without loss, while the optical sensor signal created by the sensing tip travels backward to the optical detection port without leakage into the optical source port. However, to the best of our knowledge, there has been no report of a POF coupler satisfying this requirement.

This study investigated both theoretically and experimentally an asymmetric 1×2 plastic fiber coupler for a POF sensor system. An angle polished plastic fiber (APPF) was attached to the side of the main plastic fiber (MPF). The core size of the MPF was considerably larger than that of the APPF. The structure of the coupler was similar to the beam combiners [5-7], which

*Corresponding author: kgim@chonnam.ac.kr

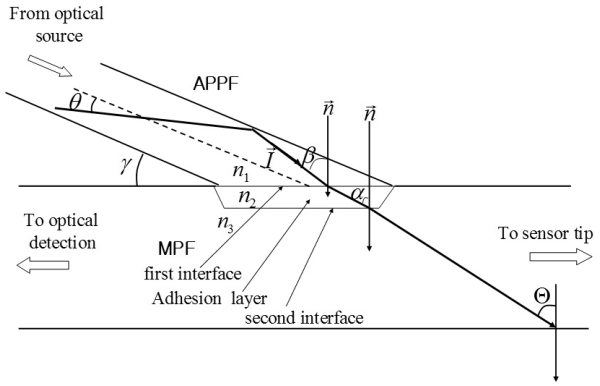


FIG. 1. Structure of the proposed asymmetric POF coupler

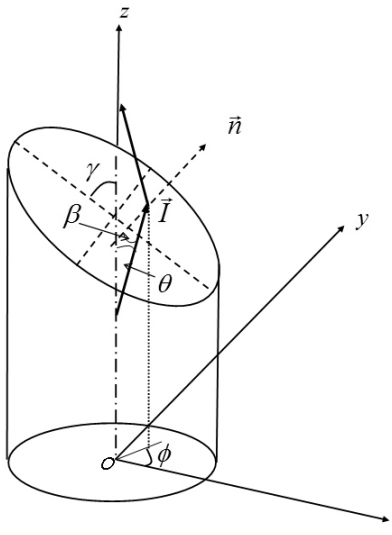


FIG. 2. End of the APPF and the coordinates

are constructed from silica fiber for a high power fiber laser. A theoretical study on the forward coupling ratio from the APPF to MPF, and backward coupling ratio from the MTF to APPF was carried out based on the geometrical optics. The influence of the device geometry on the characteristics of the coupler was analyzed. Couplers with various coupling structures were fabricated and characterized.

## II. THEORETICAL CONSIDERATION

We employed the geometrical optics to calculate theoretically the forward and backward coupling ratios because the core diameter of the plastic fiber is much larger than an optical wavelength. The optical absorption in the epoxy layer used for combining the APPF and the MPF was neglected. The thickness of the adhesion layer was assumed to be uniform and much larger than the wavelength. Therefore, the evanescent field coupling was not taken into consideration.

Figure 1 shows the configuration of the asymmetric plastic coupler for a POF sensor. The light source beam was launched into the APPF and then coupled to the MPF. Not all the light rays can be coupled to the MPF due to the Fresnel reflection at the two interfaces of the adhesion layer. In addition, such optical rays that transmitted through the interfaces, however, were incident on the core-cladding boundary of the MPF with a small incident angle cannot be guides by the total internal reflection. An optical sensor signal, such as fluorescence or reflected light, was created at the sensor tip attached to the end of the MPF. A part of the optical sensor signal travels back along the MPF to the optical detection port.

A typical light ray incident on the interface from the APPF is shown in Fig. 1. The symbol $\theta$ denotes the angle between the optical ray and the fiber axis. The coupling angle $\gamma$ is defined as the angle between the axis of the MPF and APPF. $\beta$ and $\alpha$ are the incident angles of an optical ray at two boundary surfaces. $\Theta$ is the incident angle of the ray on the MPF core-cladding cylindrical boundary surface. The symbols, $n_1$, $n_2$ and $n_3$, denote the refractive indices of the APPF core, adhesion layer and MPF core, respectively.

$\vec{I}$ is a unit vector in the direction of an incident ray in the APPF. In Cartesian coordinates as shown in Fig. 2, $\vec{I}$ can be expressed as follows:

$$\vec{I} = \hat{x}\cos\phi\sin\theta + \hat{y}\sin\phi\sin\theta + \hat{z}\cos\theta \tag{1}$$

The APPF axis was taken as the $z$ axis in the Fig. 2. The major axis of the elliptic interface surface lies in the $xz$ plane and its minor axis lies in $yz$ plane. $\phi$ is a skew angle, which is the angle between the $x$ axis and the projection of the ray to the $xy$ plane. The outward normal $\vec{n}$ is given by

$$\vec{n} = \hat{x}\cos\gamma + \hat{z}\sin\gamma \tag{2}$$

The incident angle $\beta$ at the first interface $\vec{I}$ is the angle between $\vec{I}$ and $\vec{n}$. From geometry

$$\cos\beta = \vec{I}\cdot\vec{n} \tag{3}$$

i.e.,

$$\beta = \arccos(\cos\phi\sin\theta\cos\gamma + \cos\theta\sin\gamma) \tag{4}$$

Based on Snell's law

$$\sin\alpha = \frac{n_1}{n_2}\sin\beta = n_{12}\sin\beta \tag{5}$$

In the second interface, Snell's law is written as follows:

$$\sin\Theta = \frac{n_2}{n_3}\sin\alpha = n_{23}\sin\alpha \tag{6}$$

where $\Theta$ is the angle of refraction at the second interface. The incident angle of the ray on the core-cladding boundary surface of the MPF, which is the same as $\Theta$, must be greater than the critical angle to experience the total internal reflection.

$$\Theta(\theta,\varphi,\gamma) > \arccos(NA_M / n_3) \tag{7}$$

where $NA_M$ is the numerical aperture of the MPF. The transmittance at the two interfaces can be expressed in terms of the Fresnel's law.

$$T_{12}^{TE} = \frac{\sin 2\beta \sin 2\alpha}{\sin^2(\beta+\alpha)} \tag{8a}$$

$$T_{12}^{TM} = \frac{\sin 2\beta \sin 2\alpha}{\sin^2(\beta+\alpha)\cos^2(\beta-\alpha)} \tag{8b}$$

$$T_{23}^{TE} = \frac{\sin 2\psi \sin 2\Theta}{\sin^2(\alpha+\Theta)} \tag{8c}$$

$$T_{23}^{TM} = \frac{\sin 2\psi \sin 2\Theta}{\sin^2(\alpha+\Theta)\cos^2(\alpha-\Theta)} \tag{8d}$$

In the above expressions, $T_{12}$ and $T_{23}$ are the transmittance at the first and at the second interface. The superscripts TE and TM stand for the TE and the TM polarization, respectively. The angles, $\alpha$, $\beta$, and are $\Theta$ functions of the ray parameters $\theta$, $\phi$, and $\gamma$. Consequently, $T_{12}$ and $T_{23}$ are also functions of $\theta$, $\phi$, and $\gamma$. We neglect the weak multiple reflection between the two interfaces and assumed that the light beam is unpolarized. The total transmittance $T(\theta,\ \phi,\ \gamma)$ is given by

$$T(\theta,\varphi,\gamma) = \frac{1}{2}\left\{T_{12}^{TE}T_{23}^{TE} + T_{12}^{TM}T_{23}^{TM}\right\} \tag{9}$$

Eq. (7) shows that not all the light in the APPF can propagate in the MPF. Therefore, the filter factor, $F(\theta,\ \phi,\ \gamma)$, is necessary for calculating the forward ratio.

$$F(\theta,\varphi,\gamma) = \begin{cases} 0, & \Theta(\theta,\varphi,\gamma) \le \arccos(NA_m / n_3) \\ 1, & \Theta(\theta,\varphi,\gamma) > \arccos(NA_m / n_3) \end{cases} \tag{10}$$

The total power launched into the MPF can be expressed as follows [6]:

$$P_{coupled} = \frac{1}{2\pi}\int_0^{\arcsin(NA_A/n_1)}\int_0^{2\pi} P(\theta,\varphi)T(\theta,\varphi,\gamma)F(\theta,\varphi,\gamma)d\varphi d\theta \tag{11}$$

where $NA_A$ is the numerical aperture of the APPF. $P(\theta,\ \phi)$ denotes the optical power distribution in the APPF.

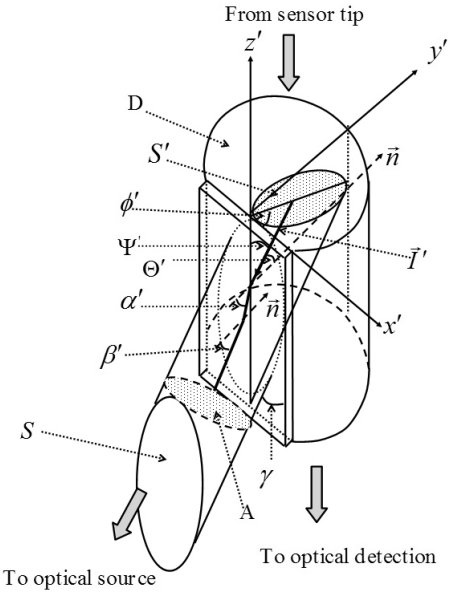


FIG. 3. Configuration of backward coupling

The total optical power in APPF is given by

$$P_{whole} = \frac{1}{2\pi}\int_0^{\arcsin(NA_A/n_1)}\int_0^{2\pi} P(\theta,\varphi)d\varphi d\theta \tag{12}$$

The coupling ratio from the APPF to the MPF can be expressed as

$$\eta_{AM} = \frac{P_{coupled}}{P_{whole}} = \frac{\frac{1}{2\pi}\int_0^{\arcsin(NA_A/n_1)}\int_0^{2\pi} P(\theta,\varphi)T(\theta,\varphi,\gamma)F(\theta,\varphi,\gamma)d\varphi d\theta}{\frac{1}{2\pi}\int_0^{\arcsin(NA_A/n_1)}\int_0^{2\pi} P(\theta,\varphi)d\varphi d\theta} \tag{13}$$

The backward coupling ratio must be suppressed because the light signal from the sensor tip propagating back to the optical source port can cause optical source instability. In order to express the trajectory of a backward ray, new Cartesian coordinates, $x'$, $y'$ and $z'$, and the cylindrical coordinates, $r'$, $\phi'$ and $z'$ were set up, as shown in Fig. 3. The $z'$ axis was parallel to the MPF axis.

The light signal generated by a sensor tip travels backward and reaches the detection port. Part of the backward signal that hits the interface area $S$ may leak into the APPF and to the optical source as shown in the Fig. 3. The shaded region $S'$ is the projection of the elliptical surface $S$ onto the $x'y'$ plane. Only those optical rays in the region $S'$ can hit the polished interface area $S$ in the direction of $\vec{I}'(\Psi',\phi')$. A backward traveling ray is defined by $\Psi'$ and $\phi'$. $\Psi'$ is the angle between the $z'$ axis and $\vec{I}'$. $\phi'$ is the skew angle between the projection of $\vec{I}'$ onto the $x'y'$ plane and the $x'$ axis. $\Theta'$ is the incident angle at the interface, which is the angle between

the normal of the interface ($\vec{n}$) and the unit propagation vector ($\vec{I}'$). In this new coordinate, $\vec{n}$ is parallel to the $y'$ axis. Hence,

$$\cos\Theta' = \sin\Psi' \sin\phi' \tag{14}$$

and

$$\Theta' = \arccos(\sin\Psi' \sin\phi') \tag{15}$$

According to Snell's law,

$$\sin\alpha' = (n_3 / n_2)\sin\Theta' = n_{32}\sin\Theta' \tag{16}$$

where $\alpha'$ is the refractive angle of the backward ray at the second interface.

The surface area $S$ of APPF is $1/\sin\gamma$ times the cross-section area $A$ of the APPF fiber,

$$S = A \ / \sin\gamma \tag{17}$$

The shaded area $S'$ is given by

$$S' = S\tan\theta' \sin\phi' \tag{18}$$

Leaky power at the coupler can be expressed as follows [7]:

$$P'_{leak} = \int_0^{\arcsin(NA_M/n_3)} \int_0^{\pi} \frac{S'}{D} P(\Psi',\phi')T'(\Psi',\phi')d\phi' d\Psi' \tag{19}$$

where $D$ is the cross section area of the MPF. $T'$ is the total transmittance at the coupler and is given by the product $T_{32}T_{21}$. The reverse transmittance, $T_{32}$ and $T_{21}$, can be obtained in the same way by use of Fresnel's law.

Not all the leaky power can be coupled back to the optical source and some rays cannot satisfy the condition required for total internal reflection of the APPF. Therefore, the filter factor is necessary for calculating the coupling ratio from the MPF to APPF.

$$F'(\Psi',\phi',\gamma) = \begin{cases} 0, & \beta'(\Psi',\phi',\gamma) \le \arccos(NA_A / n_1) \\ 1, & \beta'(\Psi',\phi',\gamma) > \arccos(NA_A / n_1) \end{cases} \tag{20}$$

The coupled power through the APPF can be written as follows:

$$P'_{coupled} = \int_0^{\arcsin(NA_M/n_3)} \int_0^{\pi} \frac{S'}{D} P'(\Psi',\phi')T'(\Psi',\phi')F'(\Psi',\phi',\gamma)d\phi' d\Psi' \tag{21}$$

The backward coupling ratio from the MPF to the APPF can be expressed as

$$\eta_{backward} = \frac{P'_{coupled}}{P'_{whole}} = \frac{1}{\sin\gamma}\frac{A}{D} \frac{\int_0^{\arcsin(NA_M/n_3)} \int_0^{\pi} P'(\Psi',\phi')T'(\Psi',\phi')F'(\Psi',\phi',\gamma)\tan\theta' \sin\phi' d\phi' d\Psi'}{\int_0^{\arcsin(NA_M/n_3)} \int_0^{2\pi} P'(\Psi',\phi')d\phi' d\Psi'} \tag{22}$$

where $P'(\Psi',\phi')$ denotes the optical power distribution in the MPF. Eq. (22), when comparing with the eq. (13), indicates that the backward coupling ratio can be controlled by changing the ratio of the core diameters of two fibers while leaving the forward coupling ratio unchanged.

## III. NUMERICAL ANALYSIS

The above theoretical model was used to simulate the propagation of light rays through the coupler. The ratio of the core diameter of the APPF to the core diameter of the MPF was 1:2. The optical power distribution in the fiber was assumed to be uniform. The index of refraction was the same for two fibers, i.e. $n_1$=$n_3$=1.49, which was taken from the reported specification for the commercial POF. The numerical aperture was 0.48 for both the APPF and the MPF.

Fig. 4 shows the dependence of the forward coupling ratio on the coupling angle $\gamma$ and refractive index of the adhesion layer $n_2$. The forward coupling ratio of the proposed coupler was strongly dependent on both parameters, $\gamma$ and $n_2$. The coupling ratio decreases with increasing coupling angle $\gamma$, because more light rays do not satisfy the total internal reflection condition and cannot be propagated along the MPF.

The highest coupling ratio was observed when the refractive indices were matched, $n_2$=$n_1$(=$n_3$), which is due to the fact of no reflection at the interfaces. As the refractive index of the adhesive layer differs from

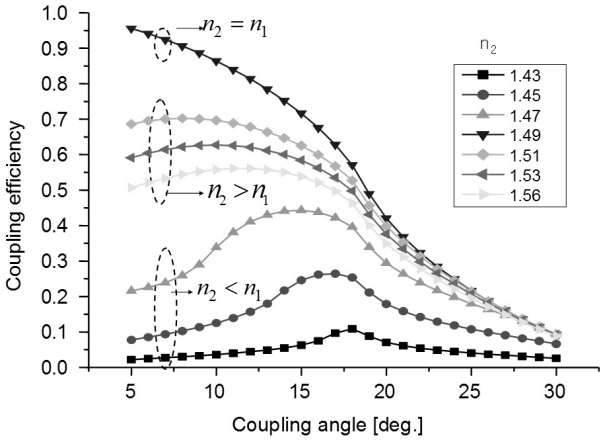


FIG. 4. Calculated forward coupling ratio in accordance with the coupling angle for various refractive indices of the adhesion layer

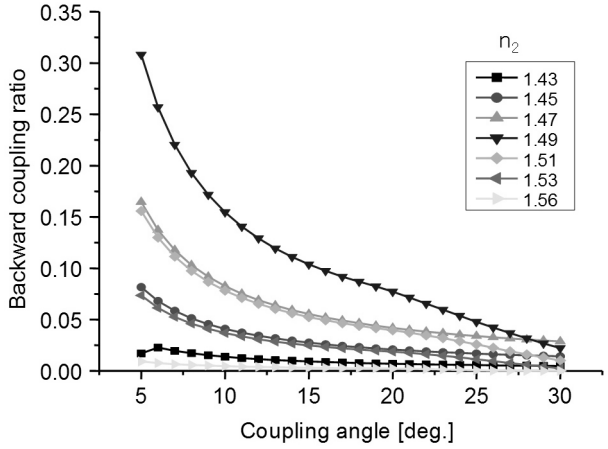


FIG. 5. Calculated backward coupling ratio in accordance with the coupling angle for various refractive indices of the adhesion layer

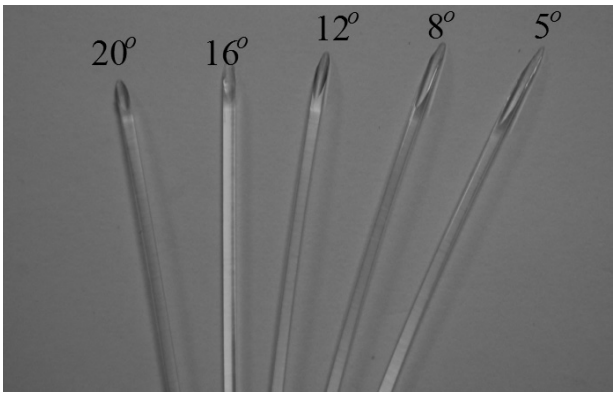


FIG. 6. Photograph of the angle polished POF

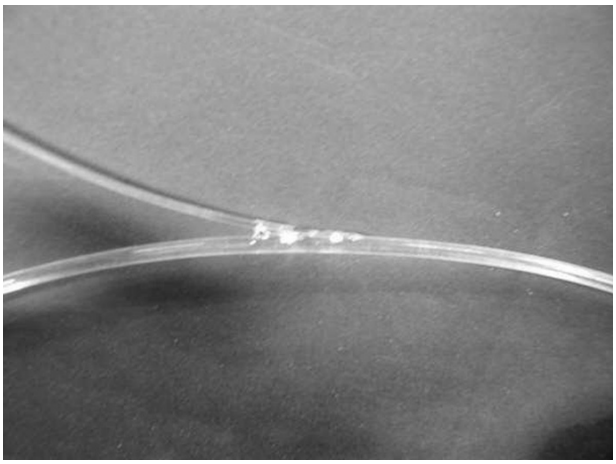

FIG. 7. A fabricated asymmetric POF coupler with 8° coupling angle

the refractive index of the POF core $n_1(=n_3)$, the coupling ratio decreases as a result of the reflection at the interfaces. In the case that $n_2$ is smaller ($n_2<n_1=n_3$), a considerable portion of rays suffer total internal reflection at the first interface. This can explain the even smaller coupling ratio in the case of $n_2<n_1$, which manifests clearly for small coupling angles, as shown in Fig. 4.

Fig. 5 shows the dependence of the backward coupling ratio on the coupling angle $\gamma$ and refractive index of the adhesive layer $n_2$. The decrease in the backward coupling ratio was attributed mainly to the ratio of the cross section area of the two fibers. As the coupling angle increases, the backward coupling ratio decreases as a result of a decrease in the interface area of the APPF ($S$), which is inversely proportional to $\sin\gamma$. In the present simulation, a small decrease in the cross sectional area of the MPF due to the side polishing was not taken into account.

On the other hand, the dependence of the backward coupling ratio on the refractive index $n_2$ is mainly due to the reflection at the interfaces. As the value of $n_2$ deviates from $n_1$, more rays become reflected at the interfaces. The effect of the total reflection in the case of $n_2<n_3$ was not manifested and only the relative index difference is significant, which is quite different from the case of the forward coupling.

A comparison of the simulation results suggests that a high forward coupling ratio from the APPF to MPF and a low backward coupling ratio from the MPF to APPF cannot be accomplished simultaneously simply by adjusting the coupling angle or refractive index of the adhesion layer. The two requirements have a trade-off relationship.

## IV. EXPERIMENTAL RESULTS

Two types of POF with different core diameters were prepared. The core diameters of the MPF and APPF were 3.0 mm and 1.5 mm, respectively. The refractive indices of the core and cladding were 1.49 and 1.41 at 630 nm, which are the same for the MPF and APPF. A number of jigs were prepared to polish the APPF with different polishing angles. APPFs with a polishing angle of 5°, 8°, 12°, 16° and 20° were fabricated. A side of the MPF was removed and polished to expose the core, and the APPF was mounted on the exposed surface of the MPF by use of adhesives. The polished area of the MPF was adjusted to the end surface area of the APPF. Fig. 6 shows the prepared polished APPFs with five different coupling angles and Fig. 7 shows the image of one of the fabricated couplers.

Two types of epoxy were used for the adhesion layer, KS-9 and NOA81, whose refractive indices were 1.49 and 1.56, respectively. A total of 10 couplers with 5 different coupling angles and 2 different refractive indices of the adhesion layer were examined. The forward and backward coupling ratios were measured using a laser diode beam with a 635 nm wavelength launched into the APPF or MPF through a multimode glass fiber.

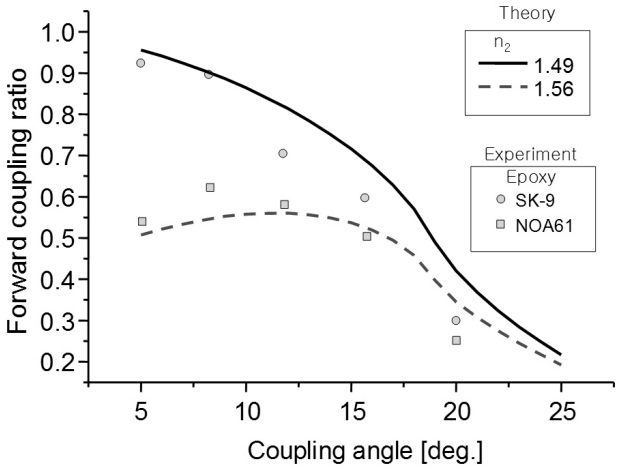


FIG. 8. Measured forward coupling ratio of the fabricated coupler

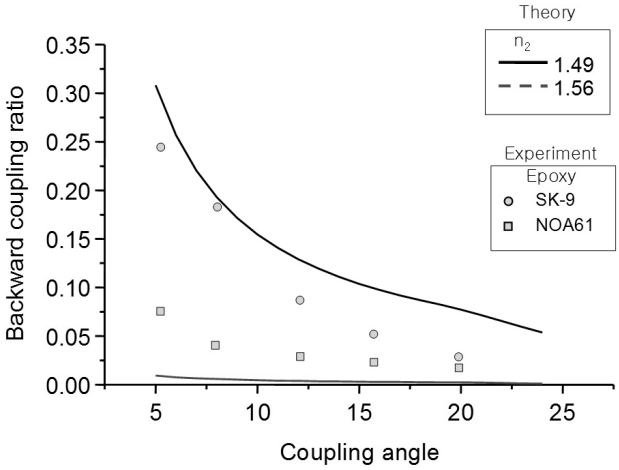


FIG. 9. Measured backward coupling ratio of the fabricated coupler

A reference POF, whose length was the same as the MPF with a coupler, was prepared for a reference coupling ratio. The coupling ratios were calibrated by comparing the measured throughput powers of the reference POF and the POF with a coupler section.

Fig. 8 shows the measured forward coupling ratios of the fabricated coupler. Although there was a slight difference between the theoretical prediction and experimental results, the overall parameter dependence of the experimental result is in good agreement with the simulation. SK-9 was adopted for the index matched epoxy. The difference between the theoretical and experimental results may be attributed to several reasons such as surface roughness of the interfaces due to imperfect fabrication process and inhomogeneous optical power distribution.

Fig. 9 shows the measured backward coupling ratios of the fabricated coupler devices. For couplers fabricated with a refractive index matched epoxy SK-9, the coupling ratios were less than the theoretical values. This could be resulted from the scattering loss at the imperfect interfaces. On the other hand, for couplers with the NOA81 epoxy, the experimentally measured values for the backward coupling ratio were much higher than the theoretical predictions. This relatively high backward coupling could be due to the scattering loss at the imperfect interfaces.

A trade-off relationship between the higher forward coupling ratio and lower backward coupling ratio was demonstrated experimentally for the structural parameters, the coupling angle and the refractive index of the adhesion layer. An asymmetric coupler with a high forward coupling ratio can be achieved easily by adopting a low coupling angle along with an index matched adhesion layer.

## V. CONCLUSION

This paper reported a side-coupled asymmetric POF coupler for optical sensors with a high forward coupling ratio and low backward coupling ratio. An angle polished POF was side-coupled into a main plastic fiber. The dependence of the coupler performance on the coupling angle between the two fibers and on the refractive index of the adhesion layer was investigated both theoretically and experimentally. A trade-off relationship between the forward coupling ratio and backward coupling ratio was found for the structural parameters, the coupling angle and the refractive index of adhesion layer. The proposed asymmetric coupler can replace the complicated optics for splitting or combining the optical source and optical sensor signal and can be used widely for fluorescence and reflection sensors.

## ACKNOWLEDGMENT

This study was supported by the Center for Photonic Materials and Devices at Chonnam National University under grant R12-2002-054. This research was also partially supported by the program for the Training of Graduate Students in Regional Innovation and the program for Regional Strategic Industries which was conducted by the Ministry of Commerce Industry and Energy, Korea.

## REFERENCE

[1] Dae-Geun Kim, Sae Yoon Woo, Dong-Kwan Kim, Seung-Han Park, and Jin-Taek Hwang, "Fabrication and Characteristics of Plastic Optical Fiber Directional Couplers," *J. Opt. Soc. Korea*, vol. 9, no. 3, pp. 99-102, 2005.

[2] J. Zubia, U. Irusta, J. Arrue, and A. Aguirre, "Design and characterization of a plastic optical fiber active

coupler," *IEEE Photon. Technol. Lett.*, vol. 10, no. 11, pp. 1578-1580, 1998.

[3] K. Imoto, H. Sano, and M. Maeda, "Plastic optical fiber star coupler," *Appl. Opt.*, vol. 25, no. 19, 3443-3447, 1986.

[4] C. Yang, X. Sun, Y. Wang, M. Zhang, and D. Ding, "1×7 plastic optical fiber coupler using cylindrical mixing rod," *Proceedings of SPIE*, vol. 4603, pp. 183-187, 2001.

[5] J. Xu, Junhua. Lu, G. Kumar, Jianren. Lu, and K. Ueda, A non-fused fiber coupler for side-pumping of double-clad fiber lasers, *Opt. Comm.*, vol. 220, no. 4-6, pp. 398-395, 2003.

[6] P. Ou, P. Yan, M. Gong, and W. Wei, "Coupling efficiency of angle-polished method for side-pumping technology," *Opt. Eng.*, vol. 43, no. 4, pp. 816-821, 2004.

[7] P. Ou, P. Yan, M. Gong, W. Wei, and Y. Yuen, "Studies of pump light leakage out of couplers for multi-coupler side-pumped Yb-doped double-clad fiber lasers," *Opt. Comm.*, vol. 239, no. 4-6, pp. 421-428. 2004.